ACS OMEGA

Article

Cite This: ACS Omega 2018, 3, 2546−2557

Peptide-Based Bioinspired Approach to Regrowing Multilayered Aprismatic Enamel

Kaushik Mukherjee,[†] Qichao Ruan,[†,∥] Steven Nutt,[‡] Jinhui Tao,[§] James J. De Yoreo,[§] and Janet Moradian-Oldak*[,†]

[†]Center for Craniofacial Molecular Biology, Division of Biomedical Sciences, Herman Ostrow School of Dentistry, University of Southern California, 2250 Alcazar Street, 90033 Los Angeles, United States

[‡]Mork Family Department of Chemical Engineering and Materials Science, University of Southern California, 3651 Watt Way, 90089 Los Angeles, United States

[§]Physical Sciences Division, Pacific Northwest National Laboratory, 902 Battelle Blvd, 99352 Richland, United States

Supporting Information

ABSTRACT: The gradual discovery of functional domains in native enamel matrix proteins has enabled the design of smart bioinspired peptides for tooth enamel mimetics and repair. In this study, we expanded upon the concept of biomineralization to design smaller amelogenin-inspired peptides with conserved functional domains for clinical translation. The synthetic peptides displayed a characteristic nanostructured scaffold reminiscent of 'nanospheres' seen in the enamel matrix and effectively controlled apatite nucleation in vitro resulting in the formation of smaller crystallites. Following application of the peptides to sectioned human molar teeth, a robust, oriented, synthetic aprismatic enamel was observed after 7 days of incubation in situ. There was a two-fold increase in the hardness and modulus of the regrown enamel-like apatite layers and an increase in the attachment of the tooth-regrown layer interface compared to control samples. Repeated peptide applications generated multiple enamel-like hydroxyapatite (HAP) layers of limited thickness produced by epitaxial growth in which *c*-axis oriented nanorods evolved on the surface of native enamel. We conclude that peptide analogues with active domains can effectively regulate the orientation of regenerated HAP layers to influence functional response. Moreover, this enamel biofabrication approach demonstrates the peptide-mediated growth of multiple microscale HAP arrays of organized microarchitecture with potential for enamel repair.

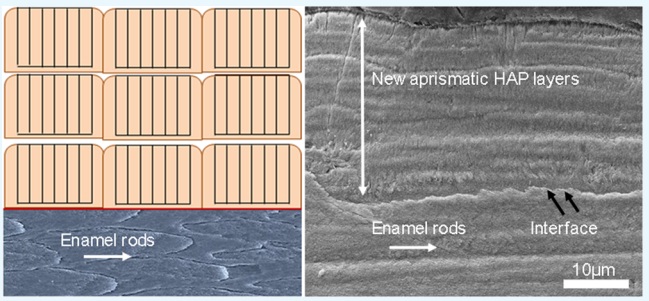

1. INTRODUCTION

Most mineralized tissues in nature are biological composites that achieve distinctive hierarchical structures through a complex integration of their mineral and organic phases across multiple length scales. Building on the principles of biomineralization, a critical understanding of material chemistry and life sciences may open trajectories for the fabrication of organized, biomimetic materials.[1−3] Dental enamel, the hardest mineralized tissue in the vertebrate body, is a biological mineralized composite characterized by an exceptional toughness and moderate brittleness that is particularly difficult to replicate synthetically. Enamel constitutes the outer protective covering of the tooth and is composed of *c*-axis oriented carbonated hydroxyapatite (HAP) nanorods (∼60 nm wide)[4] arranged in bundles of prisms or rods (∼6 μm in width)[5] and delimited by organic sheaths and interprismatic crystallites. In humans, the outermost layer of surface enamel is composed of columns of HAP crystals disposed parallel to each other and perpendicular to the enamel periphery, termed "aprismatic" or "prismless" enamel (∼16−45 μm thickness).[6] Frequently abraded during mastication, this highly mineralized aprismatic layer is harder and less permeable than the enamel subsurface.[7] This preferential use of a columnar architecture demonstrates a more regular organization of microcrystals that is associated with functionality,[8] making it an appropriate model structure to emulate for surface enamel restoration. Tooth enamel is acellular in nature, scarcely remineralizes and does not possess the capacity to remodel or regenerate. These attributes facilitate the exigency to develop enamel-inspired biomaterials for superficial repair of abraded or diseased tooth structure.

Amelogenin, the major intrinsically disordered structural protein in an enamel matrix, is believed to play a central role in enamel formation.[9−11] Previous studies have shown the in vitro assembly of amelogenin into spherical nanospheres of ∼17−18 nm diameter, which can promote crystal organization.[12,13] Amelogenin may also assemble into oligomers, nanoribbons, and other elongated assemblies under a host of different in vitro conditions.[14−16] Prior work has documented that amelogenin-

Received: December 16, 2017
Accepted: February 22, 2018
Published: March 2, 2018

DOI: 10.1021/acsomega.7b02004
ACS Omega 2018, 3, 2546−2557

based supramolecular assemblies exert a strong influence over the organization and directionality of needlelike fluoridated HAP crystals formed on the etched enamel.[17] Our knowledge of the crucial role of amelogenin in monitoring mineralization has been further developed by studying knockout mice lacking the gene that codes for amelogenin (*Amelx*). *Amelx*-null mice express a characteristic disorganized (prismless), discolored, hypomineralized enamel that is only 10−20% of normal enamel thickness and includes mixed mineral phases.[18−20] Hence, a systematic understanding of amelogenin protein structure, assembly, and behavior in a dynamic extracellular environment may lead to the design of practical peptide scaffolds for enamel mimetics. The use of peptides as an efficient fabrication strategy has facilitated the design of complex bioinspired materials and architectonics over different hierarchical length scales.[21,22] This approach offers striking benefits, such as structural programmability, biocompatibility, biodegradability, easy handling, and affordable cost of synthesis.

The growing need for minimally invasive treatment strategies to combat the increasing prevalence of tooth decay has challenged researchers and dental clinicians to reconsider a more preventive management approach. Previous studies have investigated the role of fluoride,[23,24] bioactive glasses,[25] charged amino acids,[26,27] organic scaffolds,[28,29] and dendrimers[30,31] in addressing surface enamel remineralization. Ample opportunity remains to exploit the complex assembly, active domains, and mineral precursor stabilization properties of native amelogenin protein to design a synthetic counterpart for bulk enamel restoration. Biomimetic in vitro approaches using full-length amelogenin (rP172) and leucine-rich amelogenin peptide (LRAP) have demonstrated the capacity to regrow organized enamel-like apatite crystals on demineralized tooth enamel while achieving biointegration and improved mechanical strength postenamel repair.[32−34] These treatment outcomes present advantages over conventional preventive fluoride treatments, including no risk of toxicity, offering biocompatibility, biointegration, enhanced functional responses, and improved permeation of mineral ions to treat deeper subsurface white spot lesions.[35]

Here, we report the design of two synthetic amelogenin-inspired peptides of 26 and 32 amino acid residues (P26 and P32, respectively) that retain the vital functional domains of native amelogenin. This biofabrication approach sought to characterize the designed peptides and test their potential to (a) assemble into a scaffold that may potentially control the nucleation and habit of the apatite crystalline phase, (b) reconstruct a robust synthetic aprismatic enamel in an in situ tooth model system, and (c) determine whether repeated peptide applications on tooth slices immersed in artificial saliva can be used to reconstitute organized multiple microscale layers. Such layers will be formed from nanoscale apatite crystals and will attain scalability for clinical viability. The secondary structure and assembly of the peptides were characterized using circular dichroism (CD) and transmission electron microscopy (TEM). Peptide-mediated mineralization experiments in vitro were observed using TEM and in situ Raman spectroscopy. The microstructure, orientation, elemental composition, and mechanical performance of the regenerated enamel-like HAP layers were characterized by scanning electron microscopy (SEM), energy-dispersive X-ray spectroscopy (EDXS), X-ray diffraction (XRD), and nanoindentation tests. We report a bottom-up mineralization strategy showing that amelogenin-inspired peptides with functional domains can effectively guide the oriented growth of multiple HAP layers with increased adhesion to the native enamel and increased mechanical properties.

2. RESULTS

2.1. Rationale for Peptide Design: Developing Amelogenin-Inspired Peptides for Enamel Restoration. In an attempt to develop an enamel restoration strategy with the necessary qualities for clinical adoption, we designed 26- and 32-residue amelogenin-inspired peptides (here called P26 and P32) as potential biomimetic mineralization agents based on a critical understanding of the apatite-binding and mineralization-promoting domains of the native amelogenin protein. The fundamental difference between the primary sequences of the two peptides is the presence of two extra polyproline repeat motifs (PVH/PMQ) in P32. The physicochemical properties of the peptides and their amino acid sequences are illustrated in Table 1 and Figure 1a,

Table 1. Molecular Mass, Isoelectric Point, and Physicochemical Properties of the Amelogenin-Derived Peptides P26 and P32[a]

peptide	mass (Da)	charge	IP	GRAVY
P26	3140.52	−1 (−5, +4)	4.85	−0.935
P32	3830.36	−1 (−5, +4)	5.38	−0.878

[a]Da—dalton; IP—isoelectric point; GRAVY—grand average hydropathicity.

respectively. We retained the last 12 mers of the C-terminus containing ∼50% of the charged residues of the full-length amelogenin and enriched in disorder-promoting residues (E, K, and R) that may have functional traits in promoting mineralization.[36] The close proximity of the hydrophilic C-terminus of amelogenin to the HAP surface has been directly implicated in mediating crystal nucleation and oriented growth processes through a highly specific protein−crystal interaction.[37−39] Owing to the presence of charged residues at the two end terminals of native amelogenin, both domains have proven to exert a dynamic role in their interaction with developing enamel crystals.[40] Hence, we preserved 14 amino acid residues from the inner N-terminus (residues 1−4; 16−25) with a phosphorylated serine (pS^{16}). The N-terminal plays a more active role in self-assembly and in increasing mineralization kinetics than in HAP-binding interactions, which indicate the functional diversity of separate domains within a single protein.[41] It has been shown through in vitro mineralization studies that the role on the N-terminal (+P) is to regulate the crystal shape and stabilize amorphous calcium phosphate (ACP) formation, thus playing a vital role in controlling crystal morphology and apatite phase transition.[42] For P-32, we added two polyproline repeat regions (PXX/PXQ) from the middle hydrophobic core of native amelogenin to observe whether addition of proline repeat length to the C-terminus would modulate crystal elongation and growth as suggested in previous literature.[43] The aim was to translate an in-depth understanding of the amelogenin structure and function into the design of novel amelogenin-derived peptides for regenerative studies.

2.2. P26 and P32 are Intrinsically Disordered and Form Spherical Assemblies. CD revealed that both peptides exhibited a disordered conformation (Figure 1b,c). The recorded CD spectra displayed a random-coiled structure

DOI: 10.1021/acsomega.7b02004
ACS Omega 2018, 3, 2546−2557

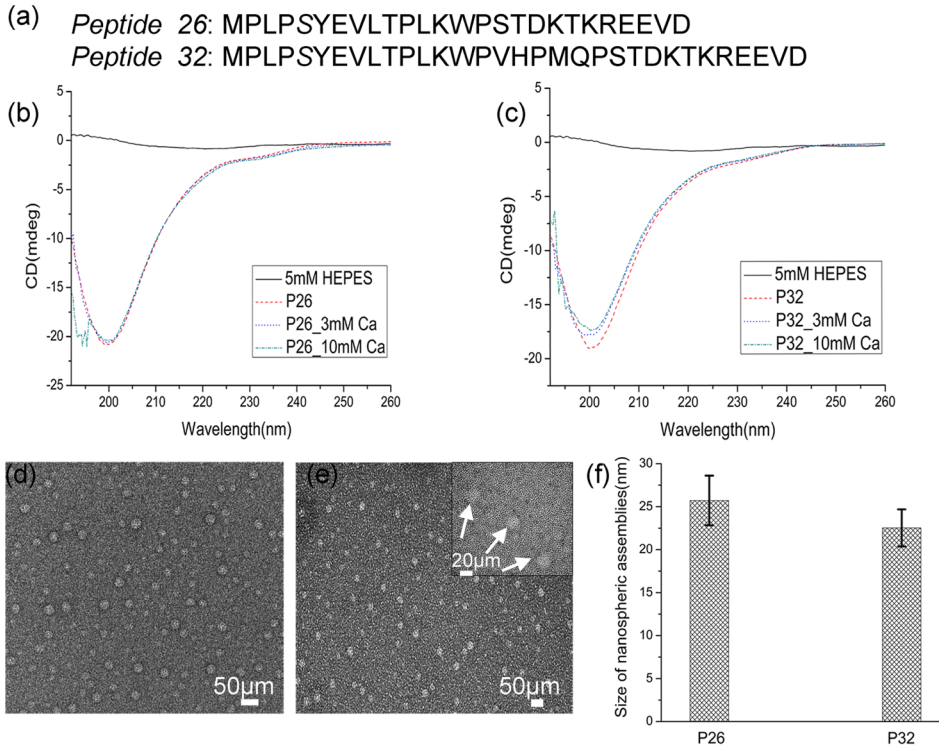

Figure 1. Structural characterization of P26 and P32 peptides: (a) amino acid sequences of peptides P26 and P32. CD spectra of peptides (0.2 mg/mL); P26 (b) and P32 (c) in 5 mM HEPES pH 7.4 at 25 °C containing 3 and 10 mM Ca^{2+}. TEM images of nanospheres formed from peptides P26 (d) and P32 (e) at pH 7.4 in HEPES buffer at 25 °C. The inset in (e) is a magnified image representative of uniformly dispersed spherical particles of peptides (white arrow) surrounded by a dense framework of threadlike nanostructures. (f) Average size distribution of the dispersed nanospheres for the two peptides calculated from the TEM images in (d,e), n = 50.

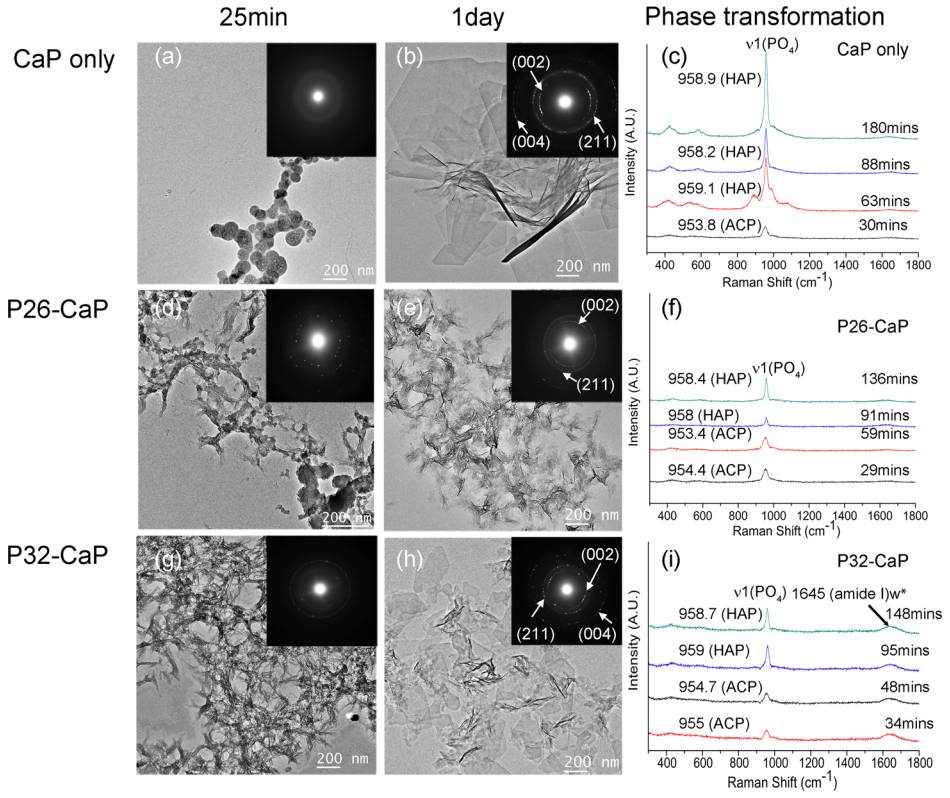

Figure 2. Ca–P mineralization in the presence of P26 and P32: TEM images, corresponding SAED images and in situ micro Raman spectroscopy analyses of mineral phases formed during in vitro mineralization experiments in the absence (a–c) and presence of (0.2 mg/mL) peptides P26 (d–f) and P32 (g–i).

DOI: 10.1021/acsomega.7b02004
ACS Omega 2018, 3, 2546–2557

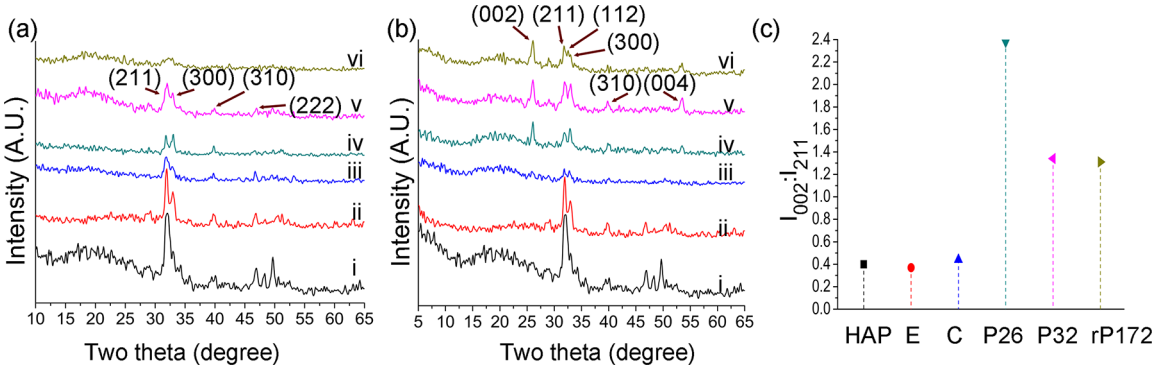

Figure 3. XRD spectra of the regenerated layers on demineralized enamel surface after 2 (a) and 7 days (b). Note an increase in the 002 diffraction signal after the 7 day peptide-treated incubation period. (c) Comparison of diffraction intensities of (002) to (211) ratios; (I_{002}/I_{211}) between different samples demonstrating an increase in *c*-axial orientation after 7 days of peptide-treatment. i—demin. enamel, ii—sound enamel, iii—control (without peptides), iv—P26, v—P32, vi—rP172. HAP—hydroxyapatite, E—sound enamel, C—control (without peptide), peptides—P26, P32, rP172—full-length recombinant amelogenin.

having a sharp negative ellipticity with a minimum at 200−205 nm. No discernible conformational changes were observed when the peptides interacted with calcium (3 and 10 mM). Full-length recombinant amelogenin (rP172) was used for comparison and displayed a random-coiled structural conformation similar to that of the peptides, consistent with previous literature.[44]

The assembled nanostructures formed by the peptides were examined by TEM. P26 and P32 displayed the formation of dispersed, characteristic nanospherical particles 25.7 ± 2.8 nm and 22.5 ± 2.15 nm in diameter, respectively (Figure 1d−f, n = 50). Single units (~3 nm diameter) organized as tiny threadlike or chainlike nanostructures formed a dense framework in the background along with the dispersed spherical assemblies (Figure 1e inset). Sample buffer (5 mM HEPES) used as a control did not yield any evident substructures (Figure S1).

2.3. P26 and P32 Controlled Apatite Crystal Nucleation and Size in Solution. Building on our findings regarding the peptide assemblies, we further investigated the effects of P26 and P32 on Ca−P mineralization in vitro using TEM (after 25 min and 24 h). In the control samples with CaP only (no peptides), spherical ACP[45] was seen within 25 min of mineralization and verified with mineral phase identification using selected-area electron diffraction (SAED) (Figure 2a). After 24 h of aging at room temperature (RT), random aggregates of large, mature, rhombohedral or rounded platelike crystals of different size and well-defined crystal edges were observed in control (length (l) = 82.3 ± 32.9 nm; maximum width of crystals was up to 800 nm, n = 55) (Figure 2b). When peptides P26 and P32 (0.2 mg/mL) were added to CaP, several agglomerates (networks) of amorphous lamellalike structures were detected after 25 min of aging (Figure 2d,g). The density of the scattered nanostructures observed on the surface of the grids was relatively higher than that of the control (without peptide) suggesting that peptides accelerated crystal nucleation. Addition of peptides resulted in the formation of smaller, thin, platelike HAP crystals of relatively uniform size distribution after 24 h of aging (Figure 2e,h). In general, the HAP particles formed in the presence of peptides were smaller than those in the control (P26 (l): 42.7 ± 13.5 nm; P32 (l): 66.2 ± 23.3 nm, n = 55, p < 0.001). The crystals formed in the presence of P26 were smaller in size than those formed in the presence of P32.

In situ Raman spectra collected continuously up to 3 h of mineralization revealed initial peaks of ACP for all three samples (Figure 2c,f,i). The peak center positions were fitted by Gaussian functions, and phase transformation (ACP to HAP) was monitored by peak shift from ~954 ± 1 to 959 ± 1.[46,47] The phase transformation start time points for the control, P26, and P32 was captured at 55.88, 64.88, and 58 min, respectively. After 90 min, HAP crystals appeared in all the samples, and the intensity for HAP peaks (~958 cm^{-1}) in control (Figure 2c) was stronger and more distinct than the mineral peaks detected in the presence of the peptides (Figure 2f,i), which in accordance with TEM may indicate presence of larger apatite crystals in control. Full-length recombinant amelogenin (rP172), used for comparison, strongly inhibited apatite formation for up to 18 h, as seen under Raman spectroscopy (Figure S2). The spectra for rP172 revealed strong amide peaks at 1255 cm^{-1} (amide III) and 1669 cm^{-1} (amide I), corroborating the presence of organic components in the in situ calcium phosphate solution. A weak amide I peak at ~1645 cm^{-1} was revealed in P32 while such a peak was not detected for P26 (Figure 2i). The low concentration (200 μg/mL) and small size of the peptides (~3.5 kDa) make it difficult to obtain strong amide peaks in Raman spectroscopy when compared to the full-length recombinant amelogenin (~25 kDa). The low amide I signal or lack of it may well be the result of differences in the binding affinity of P26 with HAP. Collectively, TEM, SAED, and in situ Raman spectroscopy analyses of sample solutions containing the peptides were similar in nature and consistent with the formation of HAP (Figure 2).

2.4. P26 and P32 Improved Preferential Orientation of Apatite Crystals Formed on Etched Enamel. XRD was used to estimate the preferential orientation of the regenerated crystals bound to the enamel surface after application of different peptides. Figure 3a depicts the tooth specimens after 2 days of peptide treatment, showing XRD peaks at 2θ = 31.8°(211), 32.8°(300), 46.7°(222), and 39.7°(310). The intensity of the diffraction peaks was calculated by a peak separation process according to Gaussian fit. After two days of peptide treatment, clear diffraction peaks at (211) and (300) were obtained that matched the peaks expected for HAP (JCPDF #09-0432). Full-length amelogenin revealed an indistinct broadened peak (~32°) lacking the characteristic diffraction pattern of HAP, indicating that the regenerated crystals lacked long-range atomic order and were in a less ordered state. This could be attributed to the role of recombinant amelogenin in stabilizing transient mineral phases

DOI: 10.1021/acsomega.7b02004
ACS Omega 2018, 3, 2546−2557

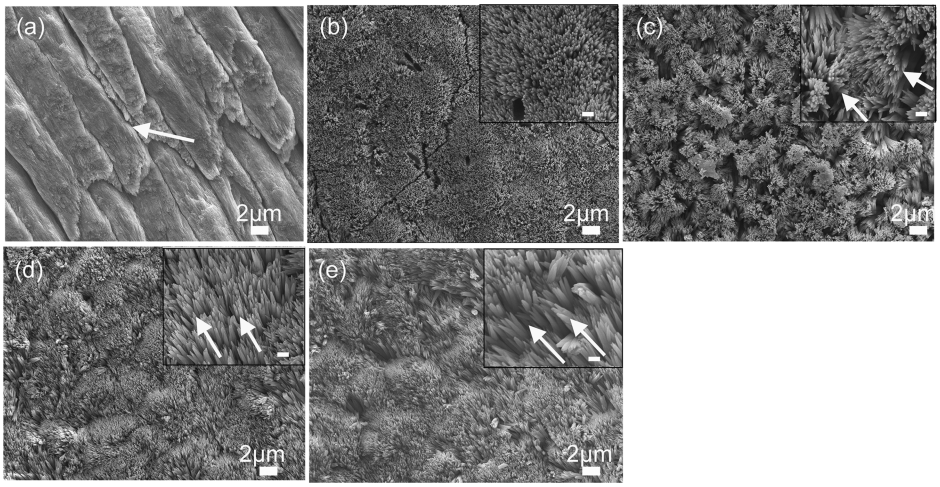

Figure 4. SEM images of (a) demineralized enamel surface showing clear outlines of enamel prisms/rods with remnants of interprismatic enamel (white arrow). (b–e) HAP crystals grown on demineralized enamel after 2 days of incubation in artificial saliva in pH 7.0 at 37 °C. Demineralized enamel treated in artificial saliva only (control) (b) in the presence of P26 (c), in P32, (d) and in rP172 (e). The insets are magnified images (scale = 500 nm). White arrows in (c) represent bundles of needlelike crystallites, whereas the arrows in (d,e) show crystallites aligned parallel to the underlying native enamel.

over a longer duration. The control sample treated in artificial saliva without peptides only showed a weak broadened (211) peak, indicating either smaller crystallite size (compared to the peptide-treated crystals) or poor crystallinity.

Figure 3b depicts the tooth specimens after 7 days of treatment, showing diffraction peaks at 2θ = 25.9°(002), 31.8°(211), 32.8°(300), and 39.8°(310). A distinct (002) peak appears in P26-, P32-, and rP172-treated samples, indicating preferential *c*-axis growth, corresponding to the long axis of the crystals and perpendicular to the enamel surface (Figure 3b). The 002 direction is the main preferential orientation for HAP crystals in bulk enamel prisms, with the *c*-axial growth along the long axis of the tooth and perpendicular to the dentin–enamel junction.[48] The ratio of the diffraction intensities (002) at 25.9° to another direction (211) was used to determine the degree of orientation along the *c*-axis. In previous studies, the intensity ratio of (002) to (211) (I_{002}/I_{211}) for random HAP (JCPDF #09-0432) was recorded at 0.4, for enamel control at 0.37, and for CaP/F/rP172 coating (calcium phosphate–fluoride–amelogenin) at 1.38.[49] After 7 days of remineralization the intensity ratios of I_{002}/I_{211} for the control, P26, P32, and rP172 groups were 0.44, 2.38, 1.34, and 1.31, respectively (Figure 3c). This finding indicates that the preferential orientation of the apatite crystals in the newly formed layer was stronger in the presence of the amelogenin-derived peptides.

2.5. P26 and P32 Promoted the Formation of Multilayered Aprismatic Crystals with Improved Mechanical Properties. After incubating the peptide-treated tooth specimens in physiologically relevant artificial saliva solution for different time periods (2 and 7 days), the morphology and the composition of the regrown apatite-containing layer was observed using SEM and EDXS. After 2 h of demineralization at pH 4.6 and at 37 °C, the enamel rods (~5 μm diameter) and remnants of the interrod material were clearly visible on the smoothened enamel surface (Figure 4a). The interprismatic enamel was demineralized, making the outlines of the prisms appear more distinct. In control enamel slices (no peptides) bathed in artificial saliva for 2 days, the crystals appeared irregular, porous, and randomly distributed, and had a low packing crystal density (Figure 4b). There was a notable difference in the uniformity of the crystal distribution and orientation between the control and peptide-treated samples.

To evaluate the orientation of the initial crystal layer grown in peptide solutions, we looked at areas of relatively low crystal density. Figure 4c shows a P26-treated sample after incubation in artificial saliva for 2 days. We observed rapid crystal overgrowth (ca. ≤100 nm width), characterized by bundles of needlelike crystals emerging perpendicular to the enamel surface and covering the entire surface of the demineralized enamel. Apatite crystals formed in the P32-treated samples for 2 days (ca. ≤100 nm width) grew parallel to the underlying prismatic enamel (Figure 4d). Here, we observed the patterning of incipient crystals along the prismatic enamel via epitaxial crystal growth. We used full-length recombinant amelogenin (rP172) for comparison in our in situ experiments (Figure 4e). The crystals regulated by the full-length protein were the longest (ca. ≥2 μm length; ca. ≤100 nm in width) and grew in a manner similar to the crystals grown with P32, that is, preferentially parallel to the long axis of the native enamel crystals. The initial distribution of the first layer of regrown crystals observed after 2 days was more heterogeneous, with some areas appearing denser than others. However, as mineralization progressed, a dense crystal layer coated the entire treated enamel surface.

To determine whether repeated peptide applications could increase the thickness of the mineralized layer, we reapplied the peptides to the tooth specimens on day 3 and observed the outcome at the end of day 7 of the remineralization cycle (n = 5 per group). Samples treated with artificial saliva only (no peptides) showed a single layer (~10 μm thickness) of randomly organized crystals that chipped easily and displayed a rough, irregular surface in the cross-sectional view. At the interface, there was no attachment to the underlying native enamel and several areas depicted porosity/irregularities in mineral formation (Figure 5a,b). The alignment of apatite crystals was poor, showing varying lengths and dimensions. rP172-treated samples demonstrated a dense coating with long, needlelike crystallites (up to 15 μm thickness) bound firmly to the underlying enamel prisms (Figure 5c,d). There was

DOI: 10.1021/acsomega.7b02004
ACS Omega 2018, 3, 2546–2557

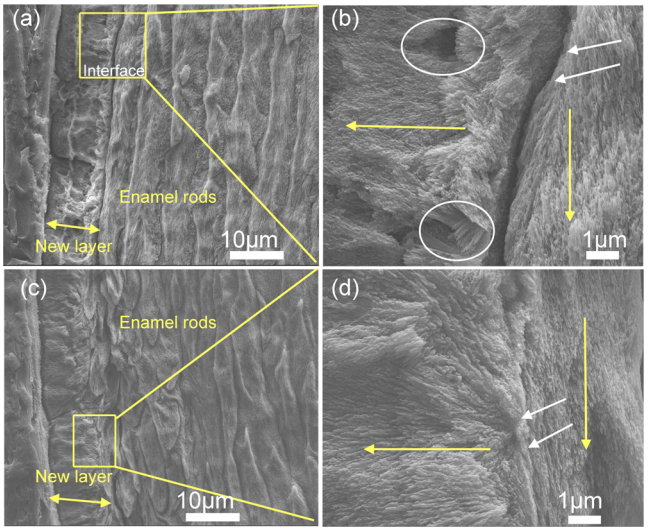

Figure 5. SEM images of the regenerated HAP layers formed on control and on rP172-treated samples after 7 days of incubation in artificial saliva in pH 7.0 at 37 °C. (a) Cross-sectional view of the control sample (without peptide) shows an irregular, roughened surface with a complete detachment at the regenerated layer−enamel interface. (b) Magnified image of the square in panel (a) displays porosities in mineral formation (white circles) with a complete loss of attachment (white arrows). (c) Cross-sectional views of samples treated in rP172 demonstrate a uniform dense, smooth coating with a seamless interface. (d) Magnified image of the square in panel (c) displays long, needlelike crystallites bound firmly to the underlying enamel prisms (white arrows).

uniformity in the thickness of the deposited crystals and, unlike the control without peptides, a smooth mineral surface was observed.

Remarkably, enamel surfaces treated with multiple applications of peptides showed a dense, continuous coating, forming multiple (2−4) columnlike apatite layers of ∼6 μm each (n = 5 samples per group). The total maximum thickness of the multilayered apatite was approximately 30 μm and grew preferentially along the apatite crystal c-axis (Figure 6a,b). Polishing and etching the tooth samples for 10 s with 37% phosphoric acid revealed multiple smaller layers of homogeneous dimensions (∼6 μm thick each), forming seamless interfaces with each other and showing few signs of delamination from the underlying enamel structure (Figure 6c,d). We observed similar growth of multilayered, columnlike, oriented mineral with an improved interface attachment on samples treated with P32. A rigorous 10 min sonication in a water bath ensured that only the crystals that were tightly bound to the enamel surface were retained and characterized. The results of EDXS analysis of three points per sample (n = 3) on the samples treated for 7 days indicated an elemental composition similar to that of healthy enamel (Figure 6e,f). The Ca/P (weight %) molar ratios of healthy enamel and demineralized enamel were 1.84 ± 0.16 and 1.88 ± 0.33, respectively. The analysis of the repaired enamel sample layers showed Ca/P (weight %) of 1.77 ± 0.88, 1.85 ± 0.86, and 1.74 ± 0.05 for P26-, P32-, and rP172-treated samples, respectively (Figure 6g).

Figure 7 shows the hardness (7a) and elastic modulus (7b) of the regenerated layers of HAP determined using nanoindentation equipment, measured parallel to the c-axis of the new crystals. Demineralizing enamel slices for 2 h resulted in significant erosion and reduction in mechanical strength. After a 7 day mineralization cycle, there was no improvement in the mechanical properties of samples treated with artificial saliva only (control). However, regenerated crystals grown in P26 exhibited a 1.7-fold increase in elastic modulus (Figure 7b) and a 1.8-fold increase in hardness (Figure 7a) compared to demineralized enamel. For tooth samples treated in P32, a 1.8-fold increase in elastic modulus and a 1.9-fold increase in hardness were observed compared to demineralized enamel. The increase in mechanical property values in peptide-treated demineralized enamel slices was statistically significant ($p \ll 0.05$). The modulus and hardness of the regenerated enamel-like layers were measured at a depth of 2 μm and were comparable to the modulus (51 ± 4.92 GPa) and hardness (2.79 ± 0.38 GPa) of sound tooth enamel (Figure 7). Both peptides exhibited improvement in mechanical properties compared to the control (without peptides) ($p < 0.001$). However, differences in modulus and hardness between the P26- and P32-treated layers were not statistically significant ($p > 0.05$).

3. DISCUSSION

The importance of developing alternative strategies for tooth enamel repair has been highlighted in dental research and clinical dentistry.[50] On the basis of in vitro investigations and animal models of enamel biomineralization, we have a better understanding of the structure, function, and assembly of enamel extracellular matrix components such as amelogenin. Our present study uses the application of rationally designed, amelogenin-inspired peptides with retained functional domains to promote regeneration of an apatitic mineralized layer on etched human tooth enamel. We demonstrate that repeated peptide applications can promote oriented nucleation of layers of apatite crystals on sectioned human molars, forming a seamless interface with the underlying native enamel. The hardness and elastic modulus of the multilayered aprismatic crystals were greater than the demineralized enamel and the layers that grew in the absence of peptides.

In developing dental enamel, the bulk of the hydrophobic macromolecular compartment in the extracellular matrix consists of amelogenin and relies on acidic hydrophilic proteins (enamelin) to initiate nucleation. In our study, the synthetic peptides demonstrated the potential to spontaneously agglomerate into stable nanospherical assemblies that formed a dense framework of threadlike structures through functional motifs in the peptide primary structure. The charged hydrophilic peptides used in the in vitro mineralization experiments were effective in controlling the formation of smaller HAP crystallites.

Three-dimensional organic scaffolds have been previously tested to target surface remineralization of HAP in enamel[28] and in bone tissues.[51] We used amelogenin-derived biomimetic peptide scaffolds to control and guide nucleation events on demineralized enamel surfaces in artificial saliva, while exercising control over the size and orientation of the developing HAP crystals by adsorbing on specific crystal surfaces. The hydrophilic inner N-terminus and C-terminus present in P26 and P32 constitute the active apatite-binding domains of amelogenin. Through binding to the surface of enamel, these functional domains generated the high degree of local supersaturation required for mineral nucleation via ionic interactions with calcium (pI < pH).[52] Fluoride, incorporated into the artificial saliva solution, likely acted in conjunction with

DOI: 10.1021/acsomega.7b02004
ACS Omega 2018, 3, 2546−2557

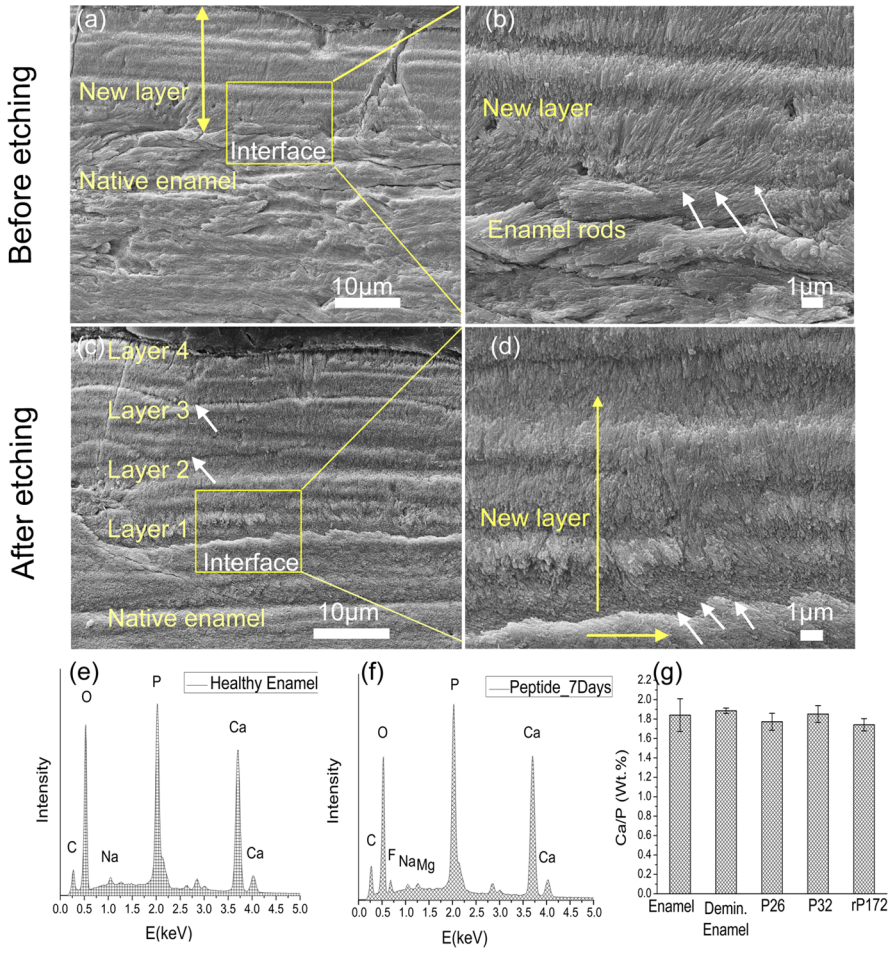

Figure 6. SEM images of the regenerated HAP layers treated in P26 after 7 days of incubation in artificial saliva in pH 7.0 at 37 °C. The artificial saliva was replenished daily, and the peptide applied on enamel slices (30 μL) on days 1 and 3. (a) Cross-sectional view of regenerated HAP layers before etching. (b) Magnified image of panel (a) (yellow square) depicts the newly formed perpendicularly stacked crystals with a seamless attachment interface with underlying enamel rods. (c) Cross-sectional view of regenerated HAP layers after etching (30% phosphoric acid, 10 s). A dense, continuous HAP coating with multiple columnar-like layers of smaller thickness dimensions is observed. (d) Magnified image of panel (c) (yellow square) depicts the presence of a continuous interface even after the etching cycle. EDXS analysis of sound enamel (e) and 7 day peptide-treated enamel surface (f) exhibited elemental peaks for Ca, P, C, Na, and O. Peptide-treated samples incubated in artificial saliva also exhibited peaks for Mg and F. (g) Ca/P content (wt %) for the various samples after the 7 day incubation cycle was found to be comparable to that of healthy enamel.

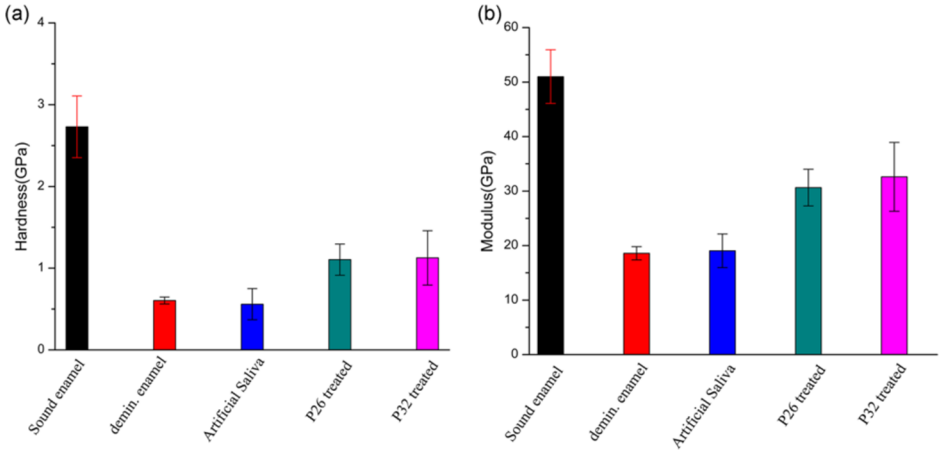

Figure 7. Nanoindentation tests showing hardness (a) and modulus (b) for sound enamel, demineralized enamel, and samples treated in control (without peptides), P26 and P32 for 7 days in artificial saliva. The error bars represent standard deviation (n = 5 per group). Demin: demineralization (2 h). Student's t-test was applied to identify differences in the hardness and elastic modulus between etched and repaired enamel ($p \leq 0.05$).

DOI: 10.1021/acsomega.7b02004
ACS Omega 2018, 3, 2546−2557

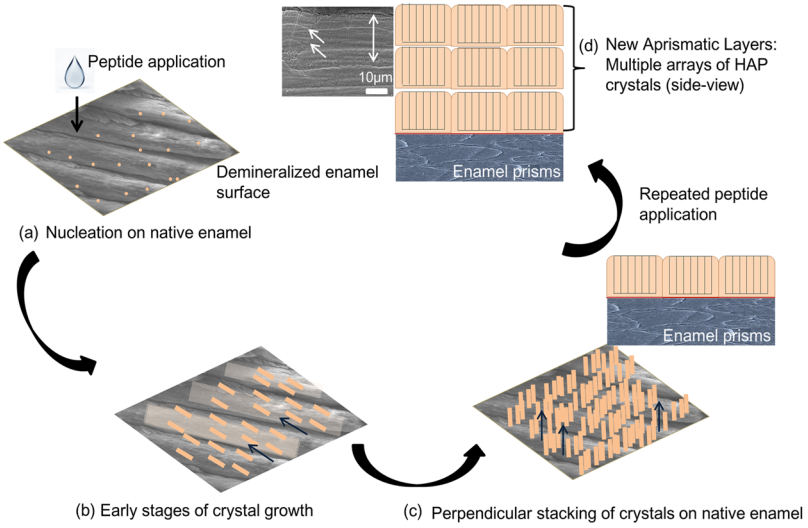

Figure 8. Schematic illustration depicting peptide-mediated regrowth of aprismatic enamel-like HAP layers on an in situ tooth model system.

the amelogenin peptides, resulting in the oriented growth of needlelike apatite crystals, as was observed previously with full-length amelogenin.[49] We observed areas where the new crystallites grew along the ends of the enamel prisms, constituting a "transition zone" to a more perpendicularly stacked crystal overgrowth. Over time, these subsequent crystalline layers exhibited an accelerated growth transition toward the *c*-axis (002), forming a columnlike layered architecture (schematically represented in Figure 8). Geometric selection phenomenon may contribute to the growth of columnar, layered structures promoted by the addition of peptides, where for each crystal unit that favors the HAP crystal to grow along their fastest growth direction (crystallographic *c*-axis).[53,54] Note that other nongeometric factors, such as direct access to fresh salivary nutrients in advance of the growing crystal interface, may also dictate texture or orientation. As the in situ remineralization cycle advanced, the crystals grew rapidly in the presence of the peptides and mutually encroached to compete for spaces and nutrients in the artificial saliva chamber. Clearly, the crystal size, morphology, and orientation within the remineralized layers were guided by the organic constituents (peptides), forming multiple smaller sublayers of limited thickness. The influence of peptides in controlling crystal dimensions was further corroborated by the in vitro experiments, where we observed smaller HAP crystal distribution in contrast to the predominantly large, heterogeneous, platelike crystals seen in the control (without peptides).

Repeated peptide application on tooth slices (on days 1 and 3 of the 7 day remineralization cycle) immersed in fresh salivary solution induced the epitaxial growth of HAP on the previously grown layers and improved the degree of orientation of the regenerated synthetic enamel. The intensity of 002 signals of HAP grown with peptides increased over the 7 day remineralization cycle. This growth mechanism led to the formation of oriented enamel-like HAP layers on the surface of the peptide-treated demineralized enamel (Figure 8). An example of competitive crystal growth in nature is the biomineralization of mollusk shells composed of aragonite or calcite crystals.[55] This type of growth pattern occurs as aragonite crystal constructs a varying microarchitecture of superimposed layers embedded in an organic framework with excellent mechanical strength and fracture toughness. A fluoride ion and D-aspartic acid formulation was used to produce multilayered *c*-axis-oriented fluorapatite nanorods on polymer sheets through geometric selection, resulting in controlled crystal dimensions via selective adsorption of aspartic acid on the *a* faces.[56]

The regenerated apatite formed by the end of the remineralization cycle in our study had a composition (i.e., Ca/P ratio) comparable to those of native enamel. The parallel arrangement of the newly formed crystallites reflected a strong resemblance to the "bandlike" or "steplike" prismless shapes seen in the outer aprismatic enamel (16−45 μm in thickness) of the permanent dentition.[6] This unique arrangement of dense crystallites oriented in parallel arrays (Figure 9) has a functional

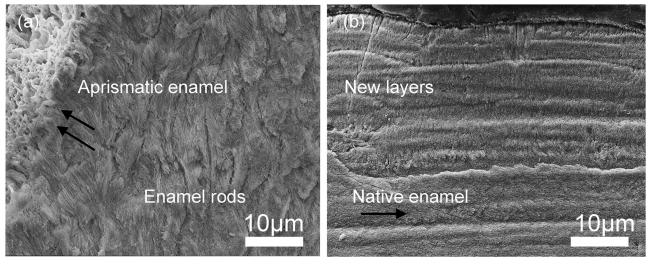

Figure 9. (a) SEM images of sound human enamel forming an outer aprismatic layer showing perpendicularly stacked HAP crystals with an orientation different from the underlying enamel rods. (b) Newly formed synthetic aprismatic enamel-like HAP layers grown in the presence of amelogenin-inspired peptide in our experiments for 7 days in situ.

role in vivo in providing fortification against acid permeability because of the absence of interprismatic spaces. Whether such protective function can be fulfilled by enamel regrown with P32 or P26 remains to be validated in future studies and will require further characterization of the regenerated layers after subjecting them to acid challenges. Even if P26 resulted in smaller crystals than those grown in the presence of P32 in vitro, HAP layers grown with P32 and P26 in situ shared structural and organizational similarities. It is possible that greater proline repeats are required to cause significant changes in crystal dimensions within the newly formed layers in situ.[43] To promote prolonged adsorption of the peptides on active

DOI: 10.1021/acsomega.7b02004
ACS Omega 2018, 3, 2546−2557

dental lesions and achieve greater reproducibility, we have contemplated the feasibility of repeated applications of an antimicrobial, muco-adhesive, peptide−chitosan hydrogel in customized trays (in preparation). This prototype has been tested in previous mineralization studies using full-length amelogenin (rP172)[32] and LRAP,[33] demonstrating promise for treating incipient carious lesions.

To improve the robustness of next-generation biomimetic materials, the driving factors that influence the biomechanical strength of intricate tissues such as dental enamel must be understood. After subjecting healthy enamel slices to a harsh 2 h-long acid-treatment cycle (pH 4.6) and treating them with peptides, there was ∼2-fold increase in the mechanical properties (hardness and elastic modulus) of peptide-treated samples when compared to that of demineralized enamel. We assert that peptide-regulated oriented growth of crystals on demineralized enamel (seen in XRD) and control of crystal size may lead to increases in hardness and modulus of the newly grown mineralized layers.

The preferred orientation values at selected tooth locations (molar cusp tips and incisor edges) are dictated by nature to impart strength required to meet the mechanical needs of the teeth. That is to say, the areas of the tooth enamel that bear the highest loads are conferred with the most favorable orientation of crystals linked along their *c*-axes (aprismatic).[57] Previous studies have indicated that tooth enamel hardness may also be influenced by controlling the size of the apatite crystals grown along the *c*-axis.[58] In aging permanent teeth, we observe larger carbonated apatite (CAP) enamel crystals[59] that seem softer and less wear-resistant than smaller CAP enamel crystals.[60] Materials with smaller crystallite size impede propagation of dislocations and require greater stress to move dislocations across a grain boundary. This imparts superior yield strength and modulus to the material. Both our in vitro and in situ studies indicated the tendency of the peptides to form smaller crystallites. The role of the inverse correlation between crystal size and hardness warrants further research, as it may shed light on how peptides such as P26 and P32 regulate crystal formation, crystallinity and refine the mechanical behavior of the regenerated mineralized layers. Such efforts could potentially provide inspiration for the development of enhanced biomaterials in restorative dentistry.

4. CONCLUSIONS

Our work highlights opportunities to design bioinspired peptides for tissue engineering and repair, made possible by the discovery of functional domains within native proteins. We elucidate how amelogenin-inspired peptides with conserved domains can mediate the organized growth of aprismatic enamel-like layers in situ while providing the means to improve the mechanical response of the new layers. P32 (with two extra polyproline repeats) differed from P26 in the structural dimensions of peptide assemblies and crystal size in vitro, although in situ the two peptides produced HAP layers with similar crystal morphology and mechanical performance. Building on these findings, exploring other functional domains capable of controlling peptide assembly, crystal size, and orientation can help refine biomaterial design. Further challenges remain in attaining the level of scalability (microns to millimeters), structural hierarchy, and durability of native enamel to augment next-generation bulk materials for clinical applications.

Ultimately, a systematic understanding of enamel matrix biology with its multifaceted cooperative interactions between assembling matrix proteins, enzymes, and mineral ions can provide a valuable foundation for the development of enamel-like biomaterials associated with functionality.

5. EXPERIMENTAL SECTION

5.1. Preparation of Synthetic Peptides and Full-Length Amelogenin rP172. The rationally designed peptides, P26 and P32, were synthesized commercially at ∼95.13% purity by CHEMPEPTIDE Limited (Shanghai, China). The peptides were phosphorylated at serine-16. High-performance liquid chromatography and mass spectrometry were used for peptide purification and mass determination by the company prior to shipment (Table 1). Recombinant full-length porcine amelogenin (rP172) lacking the N-terminal methionine and the phosphate group on serine-16 was used for comparison. rP172 was expressed in *Escherichia coli* and purified as previously described.[17] The peptide and protein samples were weighed and dissolved in filtered distilled water (DDW, Optima, Fisher Scientific) to yield stock solutions of 2 mg/mL and centrifuged (8000 rpm, 2 min). The stock solutions were placed in a slow shaker for 4 h and divided into aliquots of 100 μL/tube. The aliquots were lyophilized for 12 h at −80 °C, and the final concentrations of the synthetic peptides and rP172 were 0.2 mg/tube.

5.2. Characterization of Secondary Structures by CD. Samples of P26 and P32 (0.2 mg/mL) were dissolved in 5 mM HEPES buffer at pH 7.4 for 5 min at RT. CD spectra were collected in high-transparency quartz cuvettes with a path length of 1 mm and band width of 2 nm at 25 °C in the far UV spectral range (190−250 nm) using a JASCO J-815 circular dichroic spectrometer. The experiments were conducted using the peptides in the absence and presence of calcium ions (3 and 10 mM $CaCl_2$). Conformational changes in the secondary structure of the peptides in the presence of bivalent calcium ions were investigated at pH 7.4.

5.3. Characterization of Spherical Assemblies by TEM. The peptides (0.2 mg) were dissolved in 5 mM HEPES buffer (1 mL) for 40 min, and the final pH value was adjusted to 7.4 using 1 M NaOH at RT. Peptide samples (4 μL) were applied to the surface of the grid (400 mesh carbon-coated, Ted Pella Inc, USA) for 30 s, blotted with filter paper, and rinsed with water, followed by a 20 s immersion in 2% uranyl acetate solution and air-drying. Three sets of sample grids (control with no peptides, P26, and P32) were examined using TEM (JEOL 1400) operated at 100 kV. The morphology and diameter of the assembled nanospheres were analyzed with software (Gatan Microscopy Suite).

5.4. Apatite Mineralization Experiments in the Presence of Peptides. For TEM, stock solutions of 30 mM calcium and 110 mM phosphate were prepared using reagents $CaCl_2{\cdot}2H_2O$ (ChemPure Brand) and KH_2PO_4 (EM Science). Mineralization experiments were repeated three times. The pH of the phosphate solution was adjusted to ∼7.4 at RT. All solutions were filtered three times (Millex-GV, 0.22 μm filter unit) prior to use. The samples (100 μL) of P26 and P32 were prepared at 0.2 mg/mL concentration. Aliquots of phosphate and calcium were sequentially added to the solutions to adjust the final concentrations to 3 mM Ca and 11 mM P. The high concentration of phosphate also acted as a buffer, and the initial pH values recorded for all the solutions were ∼7.24−7.34. After mixing all the components in Eppendorf tubes, the solutions

DOI: 10.1021/acsomega.7b02004
ACS Omega 2018, 3, 2546−2557

were vortexed and then centrifuged for 5 min at 10 000 rpm to remove any impurities. The mineralization experiments were stopped at 25 min and 24 h. Four microliters of the crystal suspension was placed on the surface of TEM grids after mixing and dried with filter paper from the side. Samples were imaged within 1 to 2 h as described above when operated at 200 kV. In the mineralization experiments, the majority of the apatite crystals formed an "edge-on" or "face-on" orientation on the TEM grid surface. Three sets of sample grids (control with no peptides, P26, and P32) were prepared in duplicates. Images were obtained in bright field and SAED modes using TEM (JEOL-2100) operated at 200 kV.[61] The dimension of the apatite crystals was analyzed based on an accumulative reading of 55 measurements from each set using software (Gatan Microscopy Suite, digital micrograph coupled with TEM CCD camera).

5.5. In Situ Raman Spectroscopy. Raman spectroscopy was used to investigate the mineral phase transformation during HAP crystallization in samples with and without the peptides. The concentrations of the peptides were 0.2 mg/mL at pH 7.4. The concentrations of calcium and phosphate were 1.5 and 9.5 mM, respectively. The Raman spectra were collected continuously up to 3 h, from 100 to 4000 cm^{-1} under backscattering geometry using a Raman microscope (HORIBA Scientific, Japan, equipped with LabRAM ARAMIS) operated at a resolution of 1 cm^{-1} with an excitation wavelength of 532 nm and laser power of 2.5 mW. A 60× objective with numerical aperture of 0.75 was used to focus the sample and to collect the spectra for 20 s.

5.6. Tooth Sample Preparation. Healthy human molars (extracted using standard procedures at the Herman Ostrow School of Dentistry of the University of Southern California and handled with the approval of the Institutional Review Board) were collected. Excess soft tissue deposits and calculus were removed by cleaning with a tweezer and scaling. The teeth were rinsed in 70% ethanol, placed in DDW for a 20 min sonication, and stored in diluted phosphate-buffered saline (pH 7.4) with 0.002% sodium azide (microbial inhibitor) at 4 °C for further use. Prior to running the experiments, the teeth were cut longitudinally into 2 mm thick slices with a water-cooled diamond wheel saw (MTI Corporation, SYJ 150-A, USA). The slices were sequentially polished with a series of 400−4000 grit silicon carbide papers and nylon adhesive back discs with 0.50 μm colloidal silica suspension. The polished enamel slices were thoroughly rinsed with DDW, sonicated in a water bath for 5 min, and stored in DDW at 4 °C for further use.

5.7. Enamel Regrowth on Demineralized Tooth Slices. A 3 × 2 mm window was prepared on each enamel slice by coating the remaining surfaces with acid-resistant nail varnish. The dried tooth samples were exposed to a demineralization buffer (2 mM $CaCl_2{\cdot}2H_2O$, 2 mM KH_2PO_4, 50 mM sodium acetate, and 0.879 mL acetic acid) at pH 4.6 for 2 h at 37 °C, then rinsed, and ultrasonically cleaned for 5 min to remove any remnants of a smear layer. One milliliter of calcium phosphate solution (960 μL of DW, 25 μL of 0.1 M $CaCl_2$, and 15 μL of 0.1 M Na_2HPO_4) was added to the peptide sample (0.2 mg), and the pH was adjusted to a final value of 7.2. The demineralized enamel windows were then coated with 20 μL of peptide solutions (P26, P32, and rP172) followed by drying in the desiccator for 10 min at RT. Peptide-coated tooth slices were immersed in 5 mL of artificial saliva (1.2 mM $CaCl_2{\cdot}2H_2O$, 50 mM HEPES buffer, 0.72 mM KH_2PO_4, 16 mM KCl, 4.5 mM NH_4Cl, 0.2 mM $MgCl_2{\cdot}6H_20$, and 1 ppm F) at pH 7.0 at 37 °C for up to 7 days. Repeated peptide applications were performed on days 1 and 3 of this 7 day remineralization period. The artificial saliva was replenished every 24 h. After incubation, the tooth slices were sonicated in a water bath for 10 min, rinsed with deionized water, and air-dried before examination under XRD, SEM, EDXS, and nanoindentation. In total, there were 4 groups of five samples each: control (no peptide) and those treated with P26, P32, and rP172 (for comparison).

5.8. Analysis and Imaging of the in Situ Regrown Crystals on Tooth Enamel. *5.8.1. X-ray Diffraction.* XRD (Rigaku diffractometer, Rigaku Corporation, Tokyo, Japan) with Cu Kα radiation (λ = 1.542 Å) operating at 70 kV and 50 mA with a sampling step of 0.08 and 2θ of range 5−65° was used to analyze the enamel windows (3 × 2 mm) for crystal orientation and mineral phase of the newly formed crystals.

5.8.2. Scanning Electron Microscopy. Field emission SEM (JEOL JSM-7001F, JEOL Ltd., Tokyo, Japan) imaging was used to observe the regrown crystals for structural analysis after the in situ remineralization cycle. Specimens were mounted on aluminum stubs with a carbon tape. The tooth surfaces were sputtered with Au and observed under an accelerating voltage of 10 kV. Both top−down and side views of the sectioned tooth samples were observed using SEM. Element analysis and mineral content was measured after the 7 day remineralization cycle using an energy-dispersive X-ray microanalysis detector coupled to the SEM (JEOL 7001SEM-EDX). In each sample, three measuring points were selected at 3000× magnification, with a measuring time of 200 s at 10 kV (n = 3).

To observe the cross section of the newly formed layers, the tooth slices were embedded in resin. The mold space was filled with a thin layer of self-curing polymer resin and moistened with a drop of the monomer. Each tooth section was placed parallel to the mold space to guarantee the precision of the section, and the resin was poured into the remaining space using the salt and pepper method. The resin was cured for up to 2 h at RT. The blocks were extracted from the plastic mold and a longitudinal cut was made through the window (using a diamond saw advancing at low speed). The cross sections were again sequentially polished with wet grid papers using gentle force, rinsed in ethanol, sonicated in water, and rinsed thoroughly. The samples were then prepared for SEM analysis, as described above.

5.8.3. Mechanical Properties. The hardness and elastic modulus of the peptide-mediated mineralized layers were evaluated by nanoindentation tests. A Berkovich diamond indentation tip (with a curvature less than 100 nm) was used to make indentations on the sample surface. A continuous stiffness measurement (CSM) was used to measure the hardness (strength) and the elastic modulus (stiffness) of the regrown apatite layers. The following parameters were used in CSM mode: target constant strain rate of 0.05 s^{-1}, measuring depth up to 2 μm, and the distance between the indentations maintained at 100 μm to prevent interference. Four different groups (healthy enamel, demineralized enamel, P26-, and P32-treated enamel) were measured (n = 5 per group). Twenty-five indentations were recorded for each sample. Student's t-test was applied to identify differences in the hardness and elastic modulus between etched and repaired enamel ($p \leq 0.05$). All the statistical analyses were carried out using software (Origin 8.0, Origin Lab, Northampton, MA and Microsoft Office Excel 2007).

DOI: 10.1021/acsomega.7b02004
ACS Omega 2018, 3, 2546−2557

■ ASSOCIATED CONTENT

Supporting Information

The Supporting Information is available free of charge on the ACS Publications website at DOI: 10.1021/acsomega.7b02004.

TEM data of the control sample without peptides (5 mM HEPES) at pH 7.4 at RT and in situ Raman spectroscopy analyses of mineral phases formed in the presence of rP172 (0.2 mg/mL) at pH 7.4 (PDF)

■ AUTHOR INFORMATION

Corresponding Author

*E-mail: joldak@usc.edu. Phone: +1 323 442 1759. Fax: +1 323 442 2981 (J.M.-O.).

ORCID

James J. De Yoreo: 0000-0002-9194-6699

Janet Moradian-Oldak: 0000-0001-5777-6297

Present Address

‖Ormco Corporation, 1332 S Lone Hill Ave, 91740 Glendora, United States.

Notes

The authors declare no competing financial interest.

■ ACKNOWLEDGMENTS

This study was financially supported by grants from the NIH-NIDCR R01, DE-13414, DE-020099, USC Coulter Translational Partnership Program, and the GSK-IADR (2016−2017) to J.M.-O. We would also like to thank the Physical Sciences Division, Pacific Northwest National Laboratory, Richland for training and access to the in situ Raman spectroscopy machine.

■ REFERENCES

(1) Nudelman, F.; Sommerdijk, N. A. J. M. Biomineralization as an Inspiration for Materials Chemistry. *Angew. Chem., Int. Ed.* **2012**, *51*, 6582−6596.

(2) Wegst, U. G. K.; Bai, H.; Saiz, E.; Tomsia, A. P.; Ritchie, R. O. Bioinspired structural materials. *Nat. Mater.* **2015**, *14*, 23−36.

(3) Meyers, M. A.; McKittrick, J.; Chen, P.-Y. Structural Biological Materials: Critical Mechanics-Materials Connections. *Science* **2013**, *339*, 773−779.

(4) Palmer, L. C.; Newcomb, C. J.; Kaltz, S. R.; Spoerke, E. D.; Stupp, S. I. Biomimetic Systems for Hydroxyapatite Mineralization Inspired By Bone and Enamel. *Chem. Rev.* **2008**, *108*, 4754−4783.

(5) Mortimer, K. V. The relationship of deciduous enamel structure to dental disease. *Caries Res.* **1970**, *4*, 206−223.

(6) Kodaka, T.; Kuroiwa, M.; Higashi, S. Structural and Distribution Patterns of Surface Prismless Enamel in Human Permanent Teeth. *Caries Res.* **1991**, *25*, 7−20.

(7) Gwinnett, A. J. Human Prismless Enamel and Its Influence on Sealant Penetration. *Arch. Oral Biol.* **1973**, *18*, 441.

(8) Yeom, B.; Sain, T.; Lacevic, N.; Bukharina, D.; Cha, S.-H.; Waas, A. M.; Arruda, E. M.; Kotov, A. N. Abiotic tooth enamel. *Nature* **2017**, *543*, 95−98.

(9) Beniash, E.; Simmer, J. P.; Margolis, H. C. The effect of recombinant mouse amelogenins on the formation and organization of hydroxyapatite crystals in vitro. *J. Struct. Biol.* **2005**, *149*, 182−190.

(10) Fincham, A. G.; Simmer, J. P. Amelogenin proteins of developing dental enamel. *Ciba Foundation Symposium*; John Wiley & Sons, Inc., 1997; Vol. *205*, pp 118−134.

(11) Robinson, C.; Brookes, S. J.; Bonass, W. A.; Shore, R. C.; Kirkham, J.. Enamel maturation. *Ciba Foundation Symposium*; John Wiley & Sons, Inc., 1997; Vol. *205*, pp 156−174.

(12) Fincham, A. G.; Moradian-Oldak, J.; Diekwisch, T. G. H.; Lyaruu, D. M.; Wright, J. T.; Bringas, P.; Slavkin, H. C. Evidence for Amelogenin Nanospheres as Functional Components of Secretory-Stage Enamel Matrix. *J. Struct. Biol.* **1995**, *115*, 50−59.

(13) Moradian-Oldak, J.; Leung, W.; Fincham, A. G. Temperature and pH-dependent supramolecular self-assembly of amelogenin molecules: A dynamic light-scattering analysis. *J. Struct. Biol.* **1998**, *122*, 320−327.

(14) Tarasevich, B. J.; Lea, S.; Bernt, W.; Engelhard, M. H.; Shaw, W. J. Changes in the Quaternary Structure of Amelogenin When Adsorbed onto Surfaces. *Biopolymers* **2009**, *91*, 103−107.

(15) Chen, C.-L.; Bromley, K. M.; Moradian-Oldak, J.; DeYoreo, J. J. In situ AFM Study of Amelogenin Assembly and Disassembly Dynamics on Charged Surfaces Provides Insights on Matrix Protein Self-Assembly. *J. Am. Chem. Soc.* **2011**, *133*, 17406−17413.

(16) Carneiro, K. M. M.; Zhai, H.; Zhu, L.; Horst, J. A.; Sitlin, M.; Nguyen, M.; Wagner, M.; Simpliciano, C.; Milder, M.; Chen, C.-L.; Ashby, P.; Bonde, J.; Li, W.; Habelitz, S. Amyloid-like ribbons of amelogenins in enamel mineralization. *Sci. Rep.* **2016**, *6*, 23105.

(17) Fan, Y.; Sun, Z.; Wang, R.; Abbott, C.; Moradian-Oldak, J. Enamel inspired nanocomposite fabrication through amelogenin supramolecular assembly. *Biomaterials* **2007**, *28*, 3034−3042.

(18) Gibson, C. W.; Yuan, Z.-A.; Hall, B.; Longenecker, G.; Chen, E.; Thyagarajan, T.; Sreenath, T.; Wright, J. T.; Decker, S.; Piddington, R.; Harrison, G.; Kulkarni, A. B. Amelogenin-deficient mice display an amelogenesis imperfecta phenotype. *J. Biol. Chem.* **2001**, *276*, 31871−31875.

(19) Smith, C. E.; Hu, Y.; Hu, J. C.-C.; Simmer, J. P. Ultrastructure of early amelogenesis in wild-type, Amelx-/-, and Enam-/- mice: enamel ribbon initiation on dentin mineral and ribbon orientation by ameloblasts. *Mol. Genet. Genomics* **2016**, *4*, 662−683.

(20) Hu, Y.; Smith, C. E.; Cai, Z.; Donnelly, L. A.-J.; Yang, J.; Hu, J. C.-C.; et al. Enamel ribbons, surface nodules, and octacalcium phosphate in C57BL/6 Amelx(-/-) mice and Amelx(+/-) lyonization. *Mol. Genet. Genomics* **2016**, *4*, 641−661.

(21) Wang, J.; Liu, K.; Xing, R.; Yan, X. Peptide self-assembly: thermodynamics and kinetics. *Chem. Soc. Rev.* **2016**, *45*, 5589−5604.

(22) Whitesides, G. M.; Boncheva, M. Beyond molecules: Self-assembly of mesoscopic and macroscopic components. *Proc. Natl. Acad. Sci. U.S.A.* **2002**, *99*, 4769−4774.

(23) Yin, Y.; Yun, S.; Fang, J.; Chen, H. Chemical regeneration of human tooth enamel under near-physiological conditions. *Chem. Commun.* **2009**, 5892−5894.

(24) Fan, Y.; Sun, Z.; Moradian-Oldak, J. Effect of Fluoride on the Morphology of Calcium Phosphate Crystals Grown on Acid-Etched Human Enamel. *Caries Res.* **2009**, *43*, 132−136.

(25) Dong, Z.; Chang, J.; Zhou, Y.; Lin, K. In vitro remineralization of human dental enamel by bioactive glasses. *J. Mater. Sci.* **2011**, *46*, 1591−1596.

(26) Li, L.; Mao, C.; Wang, J.; Xu, X.; Pan, H.; Deng, Y.; Gu, X.; Tang, R. Bio-Inspired Enamel Repair via Glu-Directed Assembly of Apatite Nanoparticles: an Approach to Biomaterials with Optimal Characteristics. *Adv. Mater.* **2011**, *23*, 4695−4701.

(27) Wang, H.; Xiao, Z.; Yang, J.; Lu, D.; Kishen, A.; Li, Y.; Chen, Z.; Que, K.; Zhang, Q.; Deng, X.; Yang, X.; Cai, Q.; Chen, N.; Cong, C.; Guan, B.; Li, T.; Zhang, X. Oriented and Ordered Biomimetic Remineralization of the Surface of Demineralized Dental Enamel Using HAP@ACP Nanoparticles Guided by Glycine. *Sci. Rep.* **2017**, *7*, 40701.

(28) Kirkham, J.; Firth, A.; Vernals, D.; Boden, N.; Robinson, C.; Shore, R. C.; Brookes, S. J.; Aggeli, A. Self-assembling peptide scaffolds promote enamel remineralization. *J. Dent. Res.* **2007**, *86*, 426−430.

(29) Huang, Z.; Newcomb, C. J.; Bringas, P.; Stupp, S. I.; Snead, M. L. Biological synthesis of tooth enamel instructed by an artificial matrix. *Biomaterials* **2010**, *31*, 9202−9211.

(30) Chen, M.; Yang, J.; Li, J.; Liang, K.; He, L.; Lin, Z.; Chen, X.; Ren, X.; Li, J. Modulated regeneration of acid-etched human tooth enamel by a functionalized dendrimer that is an analog of amelogenin. *Acta Biomater.* **2014**, *10*, 4437−4446.

DOI: 10.1021/acsomega.7b02004
ACS Omega 2018, 3, 2546−2557

(31) Wu, D.; Yang, J.; Li, J.; Chen, L.; Tang, B.; Chen, X.; Wu, W.; Li, J. Hydroxyapatite-anchored dendrimer for in situ remineralization of human tooth enamel. *Biomaterials* **2013**, *34*, 5036−5047.
(32) Ruan, Q.; Zhang, Y.; Yang, X.; Nutt, S.; Moradian-Oldak, J. An amelogenin-chitosan matrix promotes assembly of an enamel-like layer with a dense interface. *Acta Biomater.* **2013**, *9*, 7289−7297.
(33) Mukherjee, K.; Ruan, Q.; Liberman, D.; White, S. N.; Moradian-Oldak, J. Repairing human tooth enamel with leucine-rich amelogenin peptide-chitosan hydrogel. *J. Mater. Res.* **2016**, *31*, 556−563.
(34) Kwak, S. Y.; Litman, A.; Margolis, H. C.; Yamakoshi, Y.; Simmer, J. P. Biomimetic Enamel Regeneration Mediated by Leucine-Rich Amelogenin Peptide. *J. Dent. Res.* **2017**, *96*, 524−530.
(35) Ruan, Q.; Liberman, D.; Bapat, R.; Chandrababu, K. B.; Phark, J.-H.; Moradian-Oldak, J. Efficacy of amelogenin-chitosan hydrogel in biomimetic repair of human enamel in pH-cycling systems. *J. Biomed. Eng. Inform.* **2016**, *2*, 119−128.
(36) Tavafoghi, M.; Cerruti, M. The role of amino acids in hydroxyapatite mineralization. *J. R. Soc., Interface* **2016**, *13*, 20160462.
(37) Shaw, W. J.; Campbell, A. A.; Paine, M. L.; Snead, M. L. The COOH terminus of the amelogenin, LRAP, is oriented next to the hydroxyapatite surface. *J. Biol. Chem.* **2004**, *279*, 40263−40266.
(38) Tarasevich, B. J.; Perez-Salas, U.; Masica, D. L.; Philo, J.; Kienzle, P.; Krueger, S.; Majkrzak, C. F.; Gray, J. L.; Shaw, W. J. Neutron Reflectometry Studies of the Adsorbed Structure of the Amelogenin, LRAP. *J. Phys. Chem. B* **2013**, *117*, 3098−3109.
(39) Friddle, R. W.; Battle, K.; Trubetskoy, V.; Tao, J.; Salter, E. A.; Moradian-Oldak, J.; De Yoreo, J. J.; Wierzbicki, A. Single-Molecule Determination of the Face-Specific Adsorption of Amelogenin's C-Terminus on Hydroxyapatite. *Angew. Chem., Int. Ed.* **2011**, *50*, 7541−7545.
(40) Paine, M. L.; Snead, M. L. Protein interactions during assembly of the enamel organic extracellular matrix. *J. Bone Miner. Res.* **1997**, *12*, 221−227.
(41) Gungormus, M.; Oren, E. E.; Horst, J. A.; Fong, H.; Hnilova, M.; Somerman, M. J.; Snead, M. L.; Samudrala, R.; Tamerler, C.; Sarikaya, M. Cementomimetics-constructing a cementum-like biomineralized microlayer via amelogenin-derived peptides. *Int. J. Oral Sci.* **2012**, *4*, 69−77.
(42) Le Norcy, E.; Kwak, S.-Y.; Wiedemann-Bidlack, F. B.; Beniash, E.; Yamakoshi, Y.; Simmer, J. P.; Margolis, H. C. Potential Role of the Amelogenin N-Terminus in the Regulation of Calcium Phosphate Formation in vitro. *Cells Tissues Organs* **2011**, *194*, 188−193.
(43) Gopinathan, G.; Jin, T.; Liu, M.; Li, S.; Atsawasuwan, P.; Galang, M.-T.; Allen, M.; Luan, X.; Diekwisch, T. G. H. The expanded amelogenin polyproline region preferentially binds to apatite versus carbonate and promotes apatite crystal elongation. *Front. Physiol.* **2014**, *5*, 430.
(44) Lakshminarayanan, R.; Yoon, I.; Hegde, B. G.; Fan, D.; Du, C.; Moradian-Oldak, J. Analysis of secondary structure and self-assembly of amelogenin by variable temperature circular dichroism and isothermal titration calorimetry. *Proteins* **2009**, *76*, 560−569.
(45) Mahamid, J.; Sharir, A.; Addadi, L.; Weiner, S. Amorphous calcium phosphate is a major component of the forming fin bones of zebrafish: Indications for an amorphous precursor phase. *Proc. Natl. Acad. Sci. U.S.A.* **2008**, *105*, 12748−12753.
(46) Koutsopoulos, S. Synthesis and characterization of hydroxyapatite crystals: A review study on the analytical methods. *J. Biomed. Mater. Res., Part A* **2002**, *62*, 600−612.
(47) Habraken, W. J. E. M.; Tao, J.; Brylka, L. J.; Friedrich, H.; Bertinetti, L.; Schenk, A. S.; Verch, A.; Dmitrovic, V.; Bomans, P. H. H.; Frederik, P. M.; Laven, J.; van der Schoot, P.; Aichmayer, B.; de With, G.; DeYoreo, J. J.; Sommerdijk, N. A. J. M. Ion-association complexes unite classical and non-classical theories for the biomimetic nucleation of calcium phosphate. *Nat. Commun.* **2013**, *4*, 1507.
(48) Al-Jawad, M.; Steuwer, A.; Kilcoyne, S. H.; Shore, R. C.; Cywinski, R.; Wood, D. J. 2D mapping of texture and lattice parameters of dental enamel. *Biomaterials* **2007**, *28*, 2908−2914.
(49) Fan, Y.; Sun, Z.; Moradian-Oldak, J. Controlled remineralization of enamel in the presence of amelogenin and fluoride. *Biomaterials* **2009**, *30*, 478−483.
(50) Ruan, Q.; Moradian-Oldak, J. Amelogenin and enamel biomimetics. *J. Mater. Chem. B* **2015**, *3*, 3112−3129.
(51) Hartgerink, J. D.; Beniash, E.; Stupp, S. I. Self-assembly and mineralization of peptide-amphiphile nanofibers. *Science* **2001**, *294*, 1684−1688.
(52) Le, T. Q.; Gochin, M.; Featherstone, J. D. B.; Li, W.; DenBesten, P. K. Comparative calcium binding of leucine-rich amelogenin peptide and full-length amelogenin. *Eur. J. Oral Sci.* **2006**, *114*, 320−326.
(53) Gray, N. H. Geometric Selection in Two-Dimensional Crystal Aggregates. *J. Int. Assoc. Math. Geol.* **1984**, *16*, 91−100.
(54) Olson, T. Y.; Chernov, A. A.; Drabek, B. A.; Satcher, J. H.; Han, T. Y.-J. Experimental Validation of the Geometrical Selection Model for Hydrothermally Grown Zinc Oxide Nanowire Arrays. *Chem. Mater.* **2013**, *25*, 1363−1371.
(55) Checa, A. G.; Rodríguez-Navarro, A. B.; Esteban-Delgado, F. J. The nature and formation of calcitic columnar prismatic shell layers in pteriomorphian bivalves. *Biomaterials* **2005**, *26*, 6404−6414.
(56) Nakamura, K.; Oaki, Y.; Imai, H. Multistep crystal growth of oriented fluorapatite nanorod arrays for fabrication of enamel-like architectures on a polymer sheet. *CrystEngComm* **2017**, *19*, 669−674.
(57) Raue, L.; Gersdorff, N.; Rödiger, M.; Klein, H. New insights in prism orientation within human enamel. *Arch. Oral Biol.* **2012**, *57*, 271−276.
(58) Eimar, H.; Ghadimi, E.; Marelli, B.; Vali, H.; Nazhat, S. N.; Amin, W. M.; Torres, J.; Ciobanu, O.; Albuquerque, R. F.; Tamimi, F. Regulation of enamel hardness by its crystallographic dimensions. *Acta Biomater.* **2012**, *8*, 3400−3410.
(59) Legeros, R. Z.; Piliero, J. A.; Pentel, L. Comparative Properties of Deciduous and Permanent (Young and Old) Human-Enamel. *Gerodontology* **1983**, *62*, 1.
(60) Zheng, J.; Zhou, Z. R. Effect of age on the friction and wear behaviors of human teeth. *Tribol. Int.* **2006**, *39*, 266−273.
(61) Beniash, E.; Simmer, J. P.; Margolis, H. C. The effect of recombinant mouse amelogenins on the formation and organization of hydroxyapatite crystals in vitro. *J. Struct. Biol.* **2005**, *149*, 182−190.

DOI: 10.1021/acsomega.7b02004
ACS Omega 2018, 3, 2546−2557